# TRIGA reactor absolute neutron flux measurement using activated isotopes

A. Borio di Tigliole [a,1], A. Cammi [b], D. Chiesa [c,d], M. Clemenza [c,d], S. Manera [a], M. Nastasi [c,d], L. Pattavina [d], R. Ponciroli [b], S. Pozzi [c,d], M. Prata [a], E. Previtali [c,d,*], A. Salvini [a], M. Sisti [c,d]

[a] Laboratorio Energia Nucleare Applicata (L.E.N.A.) of the University of Pavia, Via Aselli 41, 27100, Italy
[b] Energy Department of Polytechnical University of Milan, Via La Masa 34, 20156, Italy
[c] Physics Department "G. Occhialini" of the University of Milano-Bicocca, P.zza della Scienza 3, 20126 Milano, Italy
[d] INFN Section of Milano-Bicocca, P.zza della Scienza 3, 20126, Italy

## 1. Introduction

### 1.1. TRIGA reactor description

The TRIGA (Training Research and Isotope production General Atomics) Mark II is a pool-type research reactor cooled and partly moderated by light water. Fuel consists of a uniform mixture of uranium (8% wt, enriched at 20% wt in $U$), hydrogen (1% wt) and zirconium (91% wt). The TRIGA reactor of the University of Pavia has a nominal power of 250 kW in a stationary-state operation. The core shape is a right cylinder and the volume can host 90 locations distributed along 6 concentric rings labeled as A (central thimble), B, C, D, E and F, which respectively hold 1, 6, 12, 18, 24 and 30 locations. These locations can be filled either with fuel elements (FE) or different core components like dummy elements (i.e. graphite elements), control rods, neutron sources and irradiation channels. The active dimensions of the core are 45.7 cm in diameter and 35.6 cm in height. A 30 cm thick radial graphite reflector surrounds the core while the axial reflector is provided by the fuel element itself in which two 10 cm thick graphite cylinders are located at the ends of the rod. Light water in the reactor tank also has the effect of a reflector (Merz et al., 2011) (about 46 cm in the radial direction and 60 cm minimum in the axial downward direction). The reactor

* Corresponding author. Physics Department "G. Occhialini" of the University of Milano-Bicocca, P.zza della Scienza 3, 20126 Milano, Italy. Tel.: +39 02 6448 2311.
    E-mail address: ezio.previtali@mib.infn.it (E. Previtali).
[1] Currently at IAEA, Wagramer Straße 5, Vienna 1220, Austria.

tank has a diameter of 1.98 m and a height of 6.4 m. The core reactivity is controlled by means of three absorbing rods, called SHIM, REGULATING and TRANSIENT made of boron carbide (SHIM, REG) and borated graphite (TRANS). The TRIGA current core contains two different types of fuel elements: the outer rings E and F host 49 FE(s) with aluminum cladding (101-type), while the 34 fuel rods in the inner rings are 103-type FE(s), having stainless steel cladding. The TRIGA Mark II reactor in Pavia is equipped with some irradiation facilities. Among them, two are located inside the core: the central thimble, that is an aluminum pipe 3.8 cm in diameter located at the center of the fuel rings, and the pneumatic irradiation system, named Rabbit, in the outer ring. The Lazy Susan facility is a rotary specimen rack in a circular well within the radial reflector. Recently, a new irradiation facility, named Thermal Channel, was added in the pool just outside the graphite reflector (Fig.1).

### 1.2. Flux measurement by neutron activation

The neutron activation technique for the evaluation of the flux consists in irradiating some samples with a known amount of nuclei and then measuring the *activation rate R*, i.e. the number of radioisotopes that each second are created by neutron-induced reactions. The following equation describes the relation between the neutron flux ($\phi$) and the activation rate:

$$R = \mathcal{N} \int \phi(E)\sigma(E)\mathrm{d}E$$

where $\mathcal{N}$ represents the number of precursor isotopes in the irradiated sample and $\sigma(E)$ is the activation cross section. The effective cross section ($\sigma_{\mathrm{eff}}$), i.e. the mean value of the cross section weighted for the neutron energetic distribution, can be introduced to calculate the integral flux: $\Phi_{\mathrm{tot}} \equiv \int \phi(E)\mathrm{d}E$.

$$\sigma_{\mathrm{eff}} = \frac{\int \phi(E)\sigma(E)\mathrm{d}E}{\int \phi(E)\mathrm{d}E} \quad \Phi_{\mathrm{tot}} = \frac{R}{\mathcal{N}\sigma_{\mathrm{eff}}}$$
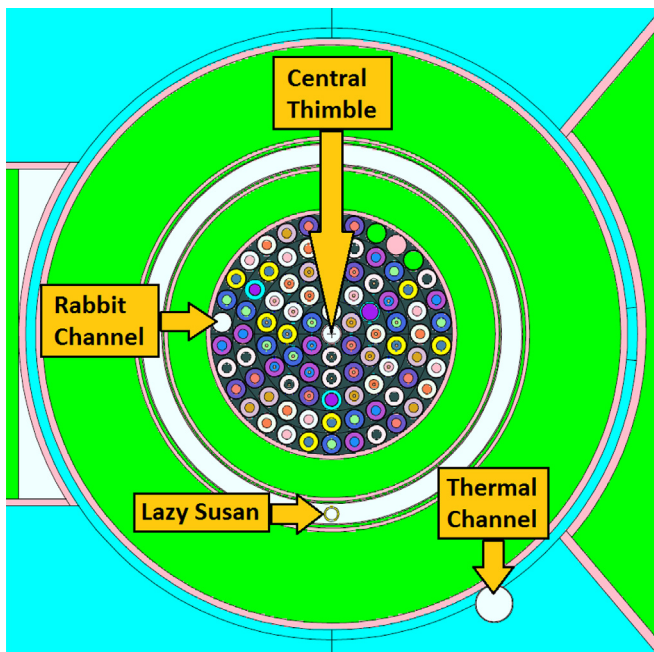


**Fig. 1.** Radial section of the TRIGA reactor core as described in the MCNP model.

**Table 1**
Masses of the irradiated samples; the experimental error is the balance sensitivity, i.e. the last decimal place.

| Sample | Central thimble | Rabbit Channel |
| --- | --- | --- |
| | Mass [mg] | Mass [mg] |
| STD 2 | 9.25 | 10.38 |
| | 51.69 | 51.01 |
| STD 3 | 9.79 | 9.71 |
| | 51.41 | 50.76 |
| STD 4 | 10.29 | 10.34 |
| | 50.90 | 47.98 |
| Fe Ni | 25.38 | 26.31 |
| | 38.42 | 44.29 |
| Ge | 77.46 | 68.39 |
| | 57.32 | 78.42 |
| In | 21.25 | 39.80 |

| Sample | Lazy Susan | Thermal Channel |
| --- | --- | --- |
| | Mass [mg] | Mass [mg] |
| STD 2 | 100.8 | 102.4 |
| STD 3 | 102.3 | 100.9 |
| STD 4 | 101.7 | 101.0 |
| Fe | 24.60 | 26.60 |
| Al–Co | – | 22.50 |
| Ni | 38.80 | 53.00 |
| Ge | 98.80 | 114.1 |
| In | 43.10 | 48.30 |

The effective cross section depends on the neutron spectrum distribution, that is different in the various irradiation facilities. For this reason, the MCNP (Briesmeister, 2005) model of the Pavia TRIGA reactor, developed and benchmarked (Borio di Tigliole et al., 2010) in the recent years, was harnessed to evaluate the neutron spectrum in the various irradiation facilities. The integral in $\sigma_{\mathrm{eff}}$ expression was numerically calculated combining the $\varphi(E)$ data from MCNP simulations with the $\sigma(E)$ data published in the ENDF/B-VII (Evaluated Nuclear Data File (ENDF)) and JEFF-3.1 (Joint Evaluated Fusion File (JEFF)) cross section libraries. We performed some tests to be sure that the number of bins (135) used for the integral calculation is large enough to obtain $\sigma_{\mathrm{eff}}$ values that are not significantly affected by the binning choice. Moreover, the $\sigma_{\mathrm{eff}}$ results obtained using the ENDF or the JEFF cross section data were compared, finding negligible differences.

When performing neutron activation, radioisotopes are mostly produced by neutron capture and they usually $\beta^-$ decay with simultaneous emission of $\gamma$-rays, even if different types of reactions and decays are possible. The activation rate is then evaluated measuring the $\gamma$-rays emitted by the isotopes to assess their activity. If the isotope after the first decay is stable, the differential equation that describes the time evolution of the radioisotope production during the irradiation is:

$$\mathrm{d}N = R\mathrm{d}t - N\lambda\mathrm{d}t \tag{1}$$

where $\lambda$ is the decay constant and $N$ the number of radioisotopes in the sample. After the irradiation, the activity of the sample is described by the following law:

**Table 2**
List of the elements in the standard solutions and mass concentration of each element.

| Standard name | Elements | Concentration [μg/mL] |
| --- | --- | --- |
| STD 2 | Sc, La, Sm, Eu, Tb, Ho, Lu, Th | 10.0 ± 1% |
| STD 3 | Cr, Co, Ga, As, Se, Ag, Cd, In, Cs, U | 10.0 ± 1% |
| STD 4 | Ru, Sb, Hf, Ir, Au | 10.0 ± 1% |

**Table 3**
List of the irradiations performed in the different facilities of the reactor. STD refers to all the multi-element standard solutions used: STD2, STD3, STD4.

| Facility | Date | Duration | Power [kW] | Samples |
|---|---|---|---|---|
| Central Thimble | 21 Nov 2011 | 2 h | 250 | STD, Fe, Ni, Ge |
| | 22 Nov 2011 | 2 h | 2.5 | In |
| Rabbit Channel | 21 Nov 2011 | 2 h | 250 | STD, Fe, Ni, Ge |
| | 10 Apr 2012 | 2 h | 250 | In |
| Lazy Susan | 11 Apr 2012 | 6 h | 250 | STD, Fe, Ni, Ge, In |
| Thermal Channel | 31 Jul 2012 | 3 h | 250 | STD, Fe, Co, Ni, Ge, In |

$$A(t) = R\left(1 - e^{-\lambda t_{irr}}\right)e^{-\lambda t}$$

where $t_{irr}$ is the irradiation time. Finally, if the measurement of a sample starts after a time $t_{wait}$ and lasts a time $t_{meas}$, the number of decays that occur is expected to be on average:

$$n_{dec} = \frac{R}{\lambda}\left(1 - e^{-\lambda t_{irr}}\right)e^{-\lambda t_{wait}}\left(1 - e^{-\lambda t_{meas}}\right)$$

Gamma-ray spectroscopy with High Purity Germanium (HPGe) detectors allows to evaluate $n_{dec}$ once the detection efficiency is known for the $\gamma$-rays emitted by each radioisotope. A Monte Carlo tool based on the GEANT4 code (Agostinelli and et al., 2003) was developed to simulate the different experimental configurations. Monte Carlo outputs give us the detector simulated energy spectra with a fixed number of decay events ($n_{sim}$) in the simulated sources. In this way, the efficiency can be evaluated as the ratio between the peaks' counts in the simulated spectra ($C_{sim}$) and $n_{sim}$ for each $\gamma$-ray of interest. Then, the number of decays ($n_{dec}$) can be calculated for each $\gamma$ line observed in the experimental spectra through the following relation:

$$n_{dec} = \frac{C_{meas}}{C_{sim}}n_{sim}$$

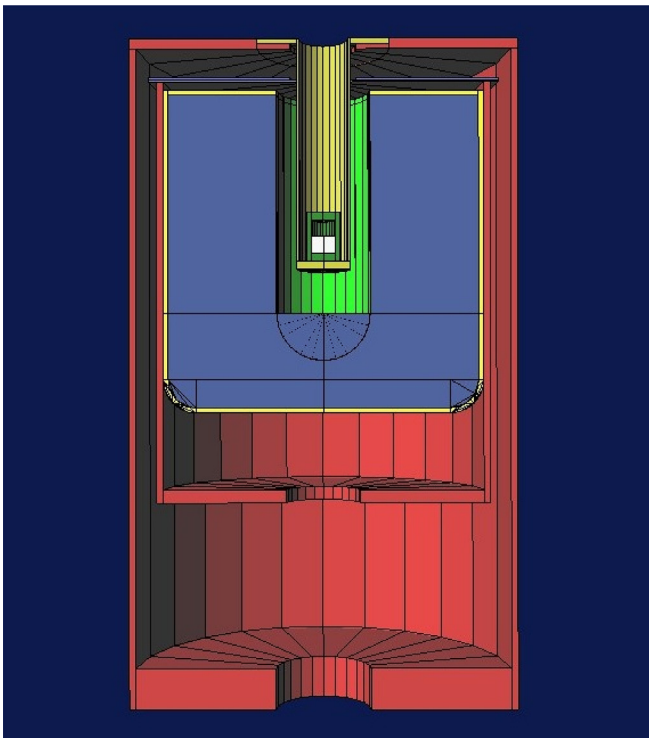where $C_{meas}$ are the peaks' counts in the recorded spectra.



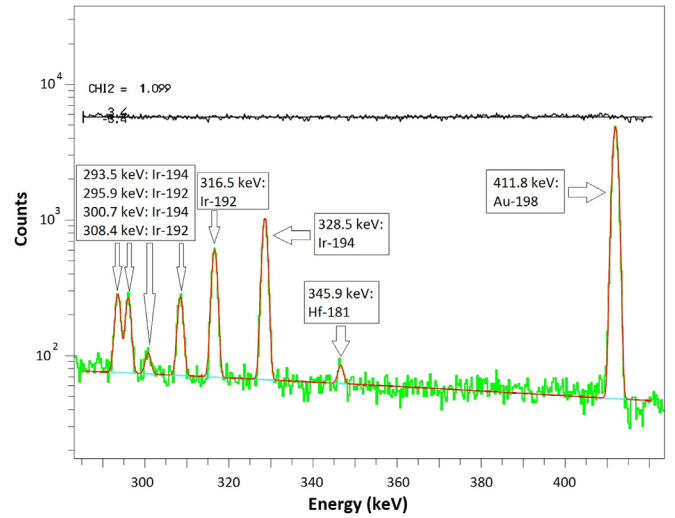**Fig. 2.** The geometric reconstruction of GePoz detector in GEANT4 simulations.



**Fig. 3.** Gaussian fit with background subtraction of some peaks in a STD4 spectrum.
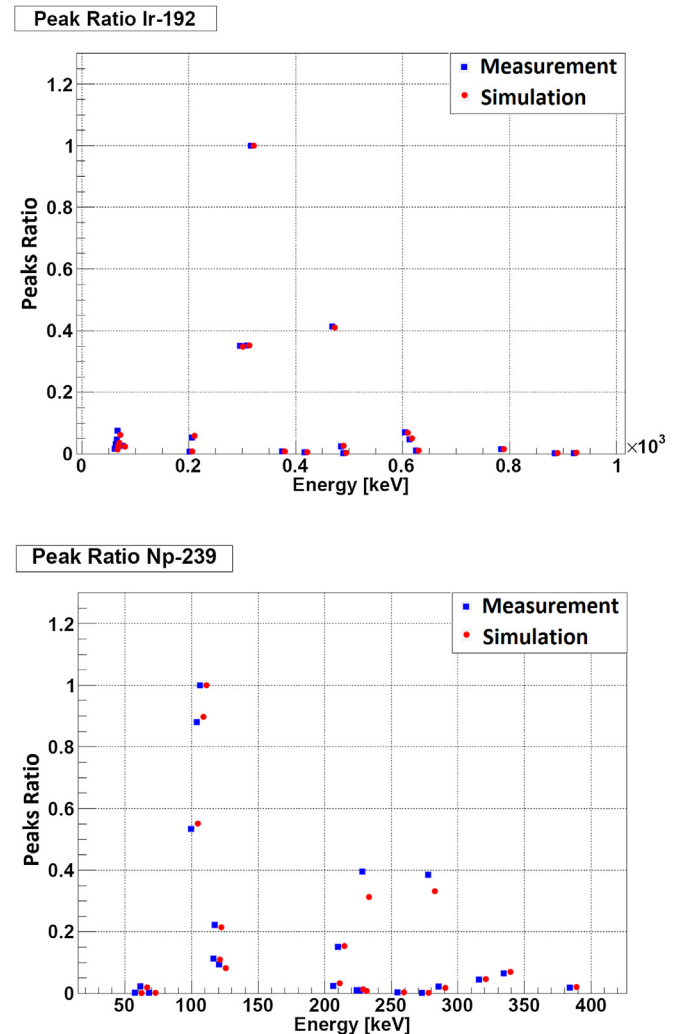


**Fig. 4.** Plot of the ratio between measurement and simulation counts of the peaks of $^{192}$Ir and $^{239}$Np.
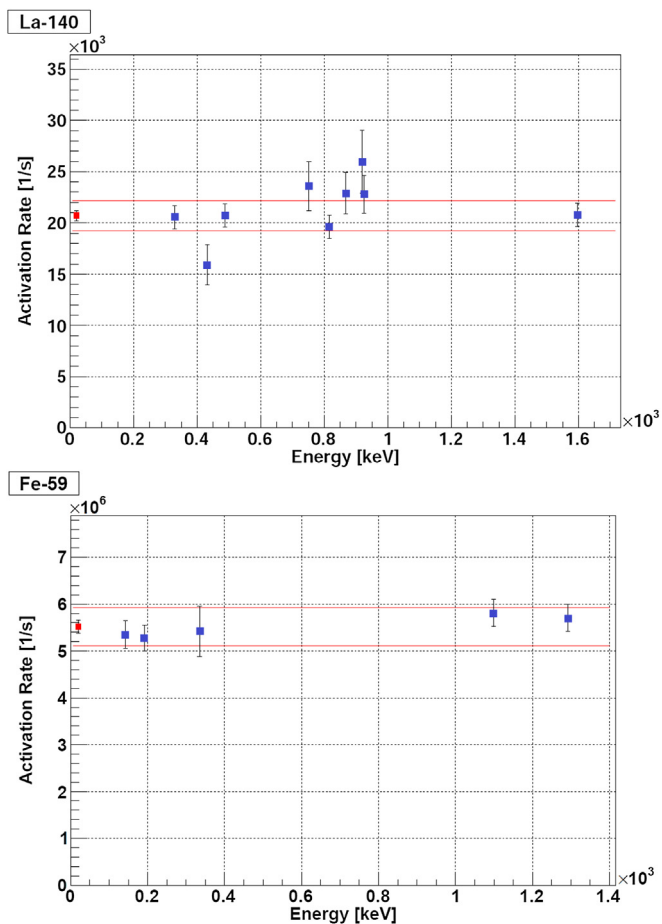
**Fig. 5.** Comparison of the results of $^{140}$La and $^{59}$Fe activation rate, calculated from the many peak data. The red point is the weighted average value. (For interpretation of the references to color in this figure legend, the reader is referred to the web version of this article.)

## 2. Irradiations and spectroscopy measurements

### 2.1. Samples irradiated

In order to obtain a very precise flux evaluation, we prepared samples containing different elements to be activated. Moreover, both liquid solutions and solid foils were used, thus diversifying the geometry and the shape of samples (Table 1). Three different Multi-element Calibration Standard solutions by PerkinElmer (Table 2), containing many elements with known concentrations, were put in polyethylene vials filled with blotting paper and their masses were measured using an analytical balance. Samples containing different mass of the same solution were prepared to control the possible systematic errors related to the weighing operations.

The irradiations were performed between November 2011 and July 2012 and lasted different times $t_{irr}$ depending on the intensity of the flux in the facility (Table 3). The reactor power level was 250 kW in all cases except for the irradiation of the Indium foil in the Central Thimble: in this case the power was decreased by a factor 100 to avoid excessive activation of the sample.

### 2.2. Measurements with HPGe detectors

The analysis of the irradiated samples was performed by means of the γ-ray spectroscopy technique, based on low background

High Purity Germanium (HPGe) detectors cooled down at 77 K. Three detectors with different features were employed:

- a coaxial Germanium with a Beryllium window (GePV);
- a coaxial Germanium with an Aluminum end-cap (GeGem);
- a well-type detector with a thin Aluminum end-cap (GePoz).

The GePV detector is installed in a shielded laboratory next to the TRIGA reactor and was used for the short measurements of the irradiated samples just after the extraction from the TRIGA reactor. The GeGem and GePoz detectors are located in the underground Radioactivity Laboratory of Milano-Bicocca University and were used for the medium and long term measurements in a low background environment (Clemenza et al., 2012). In particular, the GePoz is characterized by a high detection efficiency thanks to the well configuration where the irradiated samples are located.

Depending on the sample activity, the measurements were performed at different source-detector distances, interposing up to five hollow boxes (each 1.9 cm high), in order to have a very low dead time and limit the pile-up counts. The measurements were repeated at different $t_{wait}$ since the irradiation, in order to be sensitive to the elements with lower activity and longer decay time.

## 3. Activation rate calculation

The activation rate was evaluated for all identified isotopes in the many collected spectra[2][3]. In order to evaluate the efficiency for each measurement configuration, we decided to exploit a Monte Carlo tool, based on the GEANT4 code, for its accuracy and flexibility in simulating the particle transportation and detection. Preliminary tests were run for every detector and measurement configuration to validate the simulation tool. The experimental efficiency was evaluated through specific measurements performed with certified calibrated radioactive multi-γ sources and Monte Carlo simulations were performed to evaluate the simulated efficiency in the corresponding configuration. The two efficiencies, evaluated independently, were then compared and the detector simulation model was refined until an agreement within less than 5% was reached.

After that, the source-detector configurations of the irradiated samples' measurements were modeled with high accuracy of the details. In this respect, we underline the fact that a very precise description of the samples is crucial for a correct evaluation of the detection efficiency. Some simulation tests show that variations of few millimeters in the positions or dimensions of the samples significantly affects the efficiency parameter, because a different solid angle is subtended between the γ-ray source and the detector. For this reason, all the samples were prepared in view that a simple and precise simulation of their shape was possible. In particular, for liquid solutions, the blotting paper was used to confine the source in the lower part of the vial. Moreover, the distance between the source and the detector was measured with good accuracy and reproduced in the simulations.

The GEANT4 code includes all isotope decay schemes, so that the relative intensities of the many γ-rays emitted and the coincidence summing effect due to the γ cascades are correctly simulated. This

---

[2] With respect to Eq. (1) different formulas were used to describe the activation of G76e, because G77e decays with half-live 11.3 h on A77s, that is not stable. In this case, the activities of G77e and A77s were measured and both data were used to calculate the activation rate of G76e, finding in general a good agreement.

[3] When analyzing metastable isotopes, the probability of metastable state population after neutron capture must be introduced in the calculation of $R$. This probability was evaluated from the data on the website http://www-nts-iaea.org/ngatlas and resulted 62.5% for G77 me, 35.9% for E152 mu, 5.17% for A110 mg and 56.2% for I114 mn.
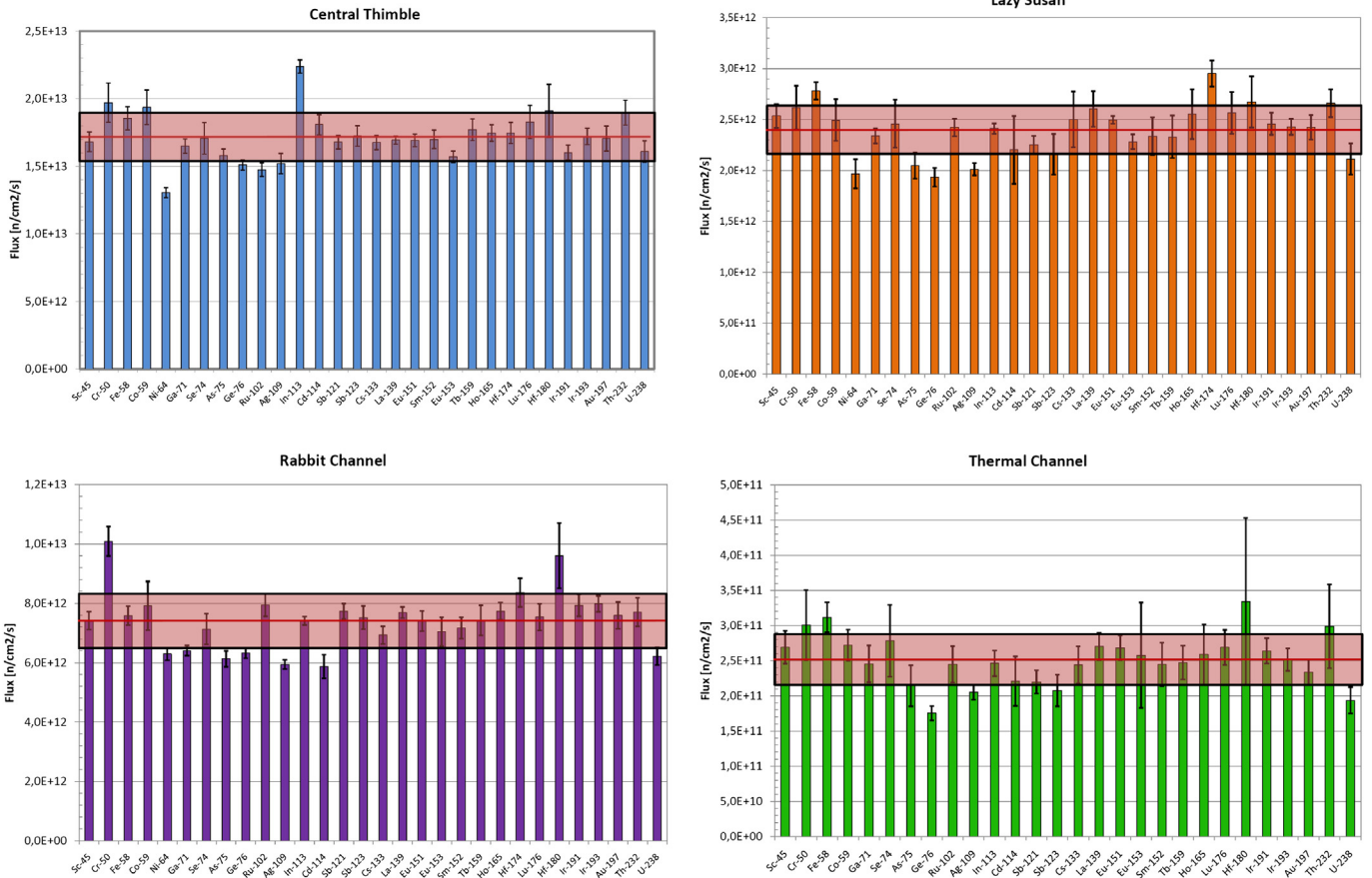
**Fig. 6.** Comparison of the neutron flux results evaluated from the data of each precursor isotope in the four irradiation facilities.

feature was crucial to analyze the measurements performed with the samples close to the detector window or inside the well of the GePoz, since in these configurations the probability of coincidence summing peaks was not negligible at all. Fig. 2

When analyzing the experimental or the simulations spectra, the number of counts in each observed peak was evaluated through a Gaussian fit, after proper subtraction of the underlying background fitted with a polynomial function (Fig.3).

When performing $\gamma$-ray spectroscopy, it is possible that different radioisotopes emit $\gamma$-rays with the same energy, thus causing peak overlapping. In order to identify these cases and correctly quantify the peak counts, a graphical tool was developed to visualize the ratios between the intensity of each line in the recorded spectra and in the corresponding simulated ones (Fig.4). When a significant discrepancy was observed for a certain peak, it was thus possible to investigate the cause (poor statistics, peaks overlapping) and exclude that peak from the analysis. The number of the excluded peaks is anyhow negligible and the overlapping lines have always been identified.

### 3.1. Use of all peaks data for a precise evaluation of R

Most radioisotopes emit many $\gamma$ and X rays and each of them can be used to calculate the activation rate ($R$). The collection of the data from many peaks allows to get a more accurate evaluation of $R$. For this purpose, it is important to consider that $\gamma$ lines are usually emitted with different intensities and the peaks' counts are known with different precision, following the Poisson statistical model. For each line, the uncertainty was calculated by combining the statistical errors in the measurement and in the simulation, plus a 5% error to

keep into account the accuracy level of the Monte Carlo models of the HPGe detectors. The activation rate for a given isotope was finally estimated as the weighted average of the different values obtained from each line in the corresponding spectrum (Fig.5).

### 3.2. Comparison of different detectors measurements

The isotopes' activation rates $R$ were separately evaluated for each detector, averaging the results of the measurements performed on the same HPGe with different configurations or $t_{meas}$. The measurements on different detectors are independent, because the geometries and the Monte Carlo models are different. When it was possible to measure the activation of an isotope with more than one detector, the independent evaluations of $R$ were compared. In general, a good agreement was found among the results, confirming the reliability of the Monte Carlo models and of the analysis method. Fig. 6

Moreover, the use of different HPGe detectors allowed to quantify the systematic error associated with a single detector and its corresponding Monte Carlo model. For each isotope measured on different detectors the standard deviation on $R$ was used to estimate these systematics.

Finally, the mean value of $R$ was calculated for each isotope and the absolute error was evaluated by matching the statistical and the systematic errors.

### 3.3. Evaluation of the specific saturation activity

The compatibility of the results from samples containing different amounts of the same elements and irradiated in the

**Table 4**
Results of the SSA of all the isotopes activated in the different irradiation facilities. The four sections include the isotopes of the STD2, STD3, STD4 and the solid samples, respectively.

| Specific saturation activity [Bq/g] | | | | |
| --- | --- | --- | --- | --- |
| Isotope | Central Thimble | Rabbit | Lazy Susan | Thermal Channel |
| **STD2** | | | | |
| $^{46}$Sc | $(2.01 \pm 0.08)10^{12}$ | $(8.97 \pm 0.35)10^{11}$ | $(3.39 \pm 0.15)10^{11}$ | $(6.86 \pm 0.59)10^{10}$ |
| $^{140}$La | $(2.30 \pm 0.03)10^{11}$ | $(1.06 \pm 0.02)10^{11}$ | $(3.98 \pm 0.27)10^{10}$ | $(7.53 \pm 0.53)10^{9}$ |
| $^{153}$Sm | $(2.37 \pm 0.09)10^{12}$ | $(1.03 \pm 0.05)10^{12}$ | $(3.66 \pm 0.28)10^{11}$ | $(4.68 \pm 0.58)10^{10}$ |
| $^{152m}$Eu | $(3.24 \pm 0.14)10^{13}$ | $(1.44 \pm 0.08)10^{13}$ | $(5.40 \pm 0.05)10^{12}$ | $(1.03 \pm 0.12)10^{12}$ |
| $^{152}$Eu | $(6.01 \pm 0.20)10^{13}$ | $(2.80 \pm 0.25)10^{13}$ | $(1.08 \pm 0.07)10^{13}$ | $(2.08 \pm 0.17)10^{12}$ |
| $^{154}$Eu | $(4.60 \pm 0.12)10^{12}$ | $(2.12 \pm 0.14)10^{12}$ | $(7.57 \pm 0.23)10^{11}$ | $(1.40 \pm 0.41)10^{11}$ |
| $^{160}$Tb | $(1.11 \pm 0.05)10^{12}$ | $(4.85 \pm 0.33)10^{11}$ | $(1.68 \pm 0.15)10^{11}$ | $(2.01 \pm 0.19)10^{10}$ |
| $^{166}$Ho | $(2.29 \pm 0.07)10^{12}$ | $(1.04 \pm 0.04)10^{12}$ | $(3.79 \pm 0.36)10^{11}$ | $(5.10 \pm 0.84)10^{10}$ |
| $^{177}$Lu | $(2.28 \pm 0.15)10^{12}$ | $(9.46 \pm 0.56)10^{11}$ | $(3.65 \pm 0.29)10^{11}$ | $(6.38 \pm 0.59)10^{10}$ |
| $^{233}$Pa | $(2.07 \pm 0.10)10^{11}$ | $(8.81 \pm 0.54)10^{10}$ | $(3.38 \pm 0.17)10^{10}$ | $(4.76 \pm 0.94)10^{9}$ |
| **STD3** | | | | |
| $^{51}$Cr | $(5.02 \pm 0.36)10^{10}$ | $(2.60 \pm 0.13)10^{10}$ | $(7.48 \pm 0.60)10^{9}$ | $(1.63 \pm 0.27)10^{9}$ |
| $^{60}$Co | $(2.68 \pm 0.18)10^{12}$ | $(1.11 \pm 0.11)10^{12}$ | $(3.88 \pm 0.31)10^{11}$ | $(7.39 \pm 0.75)10^{10}$ |
| $^{72}$Ga | $(1.29 \pm 0.04)10^{11}$ | $(5.19 \pm 0.13)10^{10}$ | $(2.10 \pm 0.06)10^{10}$ | $(3.15 \pm 0.33)10^{9}$ |
| $^{76}$As | $(3.66 \pm 0.10)10^{11}$ | $(1.48 \pm 0.06)10^{11}$ | $(5.70 \pm 0.35)10^{10}$ | $(6.78 \pm 0.92)10^{9}$ |
| $^{75}$Se | $(3.35 \pm 0.22)10^{10}$ | $(1.43 \pm 0.10)10^{10}$ | $(5.52 \pm 0.52)10^{9}$ | $(8.2 \pm 1.5)10^{8}$ |
| $^{110m}$Ag | $(1.25 \pm 0.06)10^{11}$ | $(5.12 \pm 0.11)10^{10}$ | $(1.90 \pm 0.04)10^{10}$ | $(2.35 \pm 0.12)10^{9}$ |
| $^{115}$Cd | $(1.14 \pm 0.04)10^{10}$ | $(3.96 \pm 0.26)10^{9}$ | $(1.64 \pm 0.25)10^{9}$ | $(1.23 \pm 0.20)10^{8}$ |
| $^{114m}$In | $(3.04 \pm 0.14)10^{10}$ | $(1.23 \pm 0.06)10^{10}$ | $(4.69 \pm 0.19)10^{9}$ | |
| $^{134}$Cs | $(1.40 \pm 0.04)10^{12}$ | $(6.05 \pm 0.25)10^{11}$ | $(2.40 \pm 0.26)10^{11}$ | $(2.86 \pm 0.30)10^{10}$ |
| $^{239}$Np | $(2.73 \pm 0.12)10^{11}$ | $(1.11 \pm 0.05)10^{11}$ | $(4.05 \pm 0.28)10^{10}$ | $(2.46 \pm 0.23)10^{9}$ |
| **STD4** | | | | |
| $^{103}$Ru | $(1.49 \pm 0.05)10^{10}$ | $(8.19 \pm 0.38)10^{9}$ | $(2.79 \pm 0.10)10^{9}$ | $(4.35 \pm 0.45)10^{8}$ |
| $^{122}$Sb | $(3.16 \pm 0.08)10^{11}$ | $(1.53 \pm 0.05)10^{11}$ | $(4.83 \pm 0.17)10^{10}$ | $(4.24 \pm 0.32)10^{9}$ |
| $^{124}$Sb | $(1.42 \pm 0.05)10^{11}$ | $(6.68 \pm 0.33)10^{10}$ | $(2.12 \pm 0.19)10^{10}$ | $(1.87 \pm 0.20)10^{9}$ |
| $^{175}$Hf | $(1.70 \pm 0.07)10^{10}$ | $(8.26 \pm 0.47)10^{9}$ | $(3.22 \pm 0.14)10^{9}$ | |
| $^{181}$Hf | $(1.09 \pm 0.11)10^{11}$ | $(5.59 \pm 0.64)10^{10}$ | $(1.73 \pm 0.16)10^{10}$ | $(3.7 \pm 1.3)10^{9}$ |
| $^{192}$Ir | $(7.19 \pm 0.23)10^{12}$ | $(3.62 \pm 0.16)10^{12}$ | $(1.25 \pm 0.05)10^{12}$ | $(2.19 \pm 0.15)10^{11}$ |
| $^{194}$Ir | $(2.22 \pm 0.07)10^{12}$ | $(1.08 \pm 0.03)10^{12}$ | $(3.65 \pm 0.11)10^{11}$ | $(4.83 \pm 0.30)10^{10}$ |
| $^{198}$Au | $(3.46 \pm 0.18)10^{12}$ | $(1.64 \pm 0.09)10^{12}$ | $(5.63 \pm 0.26)10^{11}$ | $(6.57 \pm 0.49)10^{10}$ |
| **Solid samples** | | | | |
| $^{59}$Fe | $(2.26 \pm 0.10)10^{8}$ | $(9.39 \pm 0.38)10^{7}$ | $(3.83 \pm 0.11)10^{7}$ | $(7.75 \pm 0.52)10^{6}$ |
| $^{60}$Co | | | | $(7.48 \pm 0.99)10^{10}$ |
| $^{65}$Ni | $(6.08 \pm 0.17)10^{8}$ | $(2.97 \pm 0.10)10^{8}$ | $(1.03 \pm 0.07)10^{8}$ | |
| $^{77}$Ge | $(7.42 \pm 0.31)10^{8}$ | $(3.13 \pm 0.19)10^{8}$ | $(1.09 \pm 0.07)10^{8}$ | $(1.27 \pm 0.10)10^{7}$ |
| $^{77}$As | $(7.89 \pm 0.20)10^{8}$ | $(3.42 \pm 0.10)10^{8}$ | $(1.18 \pm 0.08)10^{8}$ | $(1.41 \pm 0.11)10^{7}$ |
| $^{114m}$In | $(3.28 \pm 0.06)10^{10}$ | $(1.11 \pm 0.02)10^{10}$ | $(3.80 \pm 0.07)10^{9}$ | $(4.05 \pm 0.29)10^{8}$ |

Central Thimble and in the Rabbit Channel was also investigated; in fact, double samples with the same elemental composition but different masses were irradiated in these two facilities. For this reason, the activation rate per unit mass was calculated. This quantity is equal to the *specific saturation activity* (SSA), i.e. the activity of an isotope after $t_{irr} \gg \tau_{1/2}$, and its value was averaged over weight to take into account the better accuracy in the measurements of samples with larger mass. In general, the results showed a very good agreement.

In Table 4, the results of the SSA measured in all the samples activated in the four irradiation facilities are reported. It is interesting to note that two isotopes were measured both in liquid solutions and in solid samples: $^{60}$Co in Thermal Channel and $^{114m}$In in the other facilities. Since the results are compatible, this is a further confirmation that the analysis is robust and accurate.

## 4. Integral flux results

The neutron flux was finally evaluated from the activation rate results and the effective cross sections values, that were calculated thanks to the MCNP simulations of the neutron spectrum distributions in the four irradiation facilities. Some small differences were found in the effective cross section results when using the ENDF or the JEFF libraries, however these systematic errors are small when compared with the experimental error of the activation

rate measurement. In any case, the flux values were calculated with both data sets, getting to very close results.

The neutron flux results, obtained using the ENDF cross sections, are shown in Table 5 for all the analyzed radioisotopes.

For most isotopes, there is good agreement among the results: this means that the neutron energetic distributions estimated through MCNP simulations are correct and allow a precise evaluation of the effective cross sections. However, for some isotopes, significant differences are observed with respect to the mean value. Several factors may act to cause these errors: in some cases it was not possible to measure an isotope with all three detectors and the error bar does not include the systematic component, in other cases there could be uncertainties related to the isotopic abundance, the metastable state activation probability, the activation cross section or the self-shielding effect (Steinhauser et al., 2012). For this reason, the standard deviation of all isotopes flux evaluation was taken as the overall uncertainty and the flux mean value was calculated for each irradiation facility (Table 6). The relative errors of the integral fluxes are between 10% and 14%: in this respect, it is worth saying that these errors include the main systematic components, because 30 different activated isotopes were analyzed and three different HPGe detectors were employed to evaluate the activation rates.

Finally, a benchmark analysis of the MCNP simulation model was performed by comparing the measured flux values with the ones calculated through the MCNP simulations. The good

**Table 5**
Neutron flux results for all the analyzed isotopes in the four irradiation facilities.

| Precursor isotope | Central thimble $10^{13}$ n/(s cm$^2$) | Rabbit channel $10^{12}$ n/(s cm$^2$) | Lazy Susan $10^{12}$ n/(s cm$^2$) | Thermal channel $10^{11}$ n/(s cm$^2$) |
|---|---|---|---|---|
| $^{45}$Sc | 1.68 ± 0.07 | 7.41 ± 0.30 | 2.54 ± 0.12 | 2.69 ± 0.23 |
| $^{50}$Cr | 1.97 ± 0.14 | 10.10 ± 0.50 | 2.62 ± 0.21 | 3.00 ± 0.50 |
| $^{58}$Fe | 1.85 ± 0.09 | 7.58 ± 0.32 | 2.78 ± 0.09 | 3.12 ± 0.21 |
| $^{59}$Co | 1.93 ± 0.13 | 7.91 ± 0.82 | 2.49 ± 0.20 | 2.72 ± 0.22 |
| $^{64}$Ni | 1.30 ± 0.04 | 6.29 ± 0.22 | 1.97 ± 0.14 | |
| $^{71}$Ga | 1.65 ± 0.05 | 6.41 ± 0.17 | 2.34 ± 0.07 | 2.46 ± 0.26 |
| $^{74}$Se | 1.71 ± 0.12 | 7.13 ± 0.52 | 2.46 ± 0.24 | 2.78 ± 0.51 |
| $^{75}$As | 1.58 ± 0.05 | 6.13 ± 0.27 | 2.05 ± 0.13 | 2.14 ± 0.29 |
| $^{76}$Ge | 1.51 ± 0.04 | 6.32 ± 0.18 | 1.93 ± 0.09 | 1.75 ± 0.10 |
| $^{102}$Ru | 1.48 ± 0.05 | 7.94 ± 0.38 | 2.42 ± 0.09 | 2.45 ± 0.26 |
| $^{109}$Ag | 1.52 ± 0.07 | 5.93 ± 0.15 | 2.01 ± 0.06 | 2.05 ± 0.11 |
| $^{113}$In | 2.24 ± 0.05 | 7.41 ± 0.14 | 2.41 ± 0.05 | 2.46 ± 0.18 |
| $^{114}$Cd | 1.81 ± 0.07 | 5.87 ± 0.40 | 2.20 ± 0.33 | 2.21 ± 0.35 |
| $^{121}$Sb | 1.68 ± 0.05 | 7.73 ± 0.26 | 2.25 ± 0.09 | 2.20 ± 0.17 |
| $^{123}$Sb | 1.72 ± 0.08 | 7.52 ± 0.39 | 2.16 ± 0.20 | 2.08 ± 0.23 |
| $^{133}$Cs | 1.68 ± 0.05 | 6.93 ± 0.30 | 2.50 ± 0.27 | 2.44 ± 0.26 |
| $^{139}$La | 1.69 ± 0.03 | 7.68 ± 0.19 | 2.60 ± 0.18 | 2.70 ± 0.19 |
| $^{151}$Eu | 1.69 ± 0.05 | 7.40 ± 0.35 | 2.50 ± 0.04 | 2.68 ± 0.18 |
| $^{152}$Sm | 1.70 ± 0.07 | 7.17 ± 0.36 | 2.34 ± 0.18 | 2.45 ± 0.31 |
| $^{153}$Eu | 1.57 ± 0.04 | 7.04 ± 0.49 | 2.28 ± 0.07 | 2.58 ± 0.75 |
| $^{159}$Tb | 1.77 ± 0.08 | 7.42 ± 0.51 | 2.33 ± 0.21 | 2.47 ± 0.24 |
| $^{165}$Ho | 1.75 ± 0.06 | 7.73 ± 0.29 | 2.55 ± 0.24 | 2.59 ± 0.43 |
| $^{174}$Hf | 1.75 ± 0.08 | 8.36 ± 0.48 | 2.95 ± 0.13 | |
| $^{176}$Lu | 1.83 ± 0.12 | 7.53 ± 0.45 | 2.56 ± 0.20 | 2.69 ± 0.25 |
| $^{180}$Hf | 1.91 ± 0.20 | 9.6 ± 1.1 | 2.67 ± 0.25 | 3.3 ± 1.2 |
| $^{191}$Ir | 1.60 ± 0.05 | 7.93 ± 0.37 | 2.46 ± 0.11 | 2.64 ± 0.18 |
| $^{193}$Ir | 1.72 ± 0.06 | 7.98 ± 0.27 | 2.43 ± 0.08 | 2.52 ± 0.16 |
| $^{197}$Au | 1.71 ± 0.09 | 7.59 ± 0.45 | 2.42 ± 0.12 | 2.34 ± 0.18 |
| $^{232}$Th | 1.90 ± 0.09 | 7.71 ± 0.48 | 2.66 ± 0.14 | 2.99 ± 0.60 |
| $^{238}$U | 1.61 ± 0.08 | 6.22 ± 0.30 | 2.11 ± 0.15 | 1.94 ± 0.19 |

**Table 6**
Comparison between the experimental integral neutron flux and the corresponding evaluation with MCNP simulations.

| Irradiation facility | Measured flux [n/(s cm$^2$)] | Err. [%] | MCNP flux [n/(s cm$^2$)] |
|---|---|---|---|
| Central Thimble | (1.72 ± 0.17) $10^{13}$ | 10 | (1.88 ± 0.02) $10^{13}$ |
| Rabbit Channel | (7.40 ± 0.95) $10^{12}$ | 13 | (8.39 ± 0.17) $10^{12}$ |
| Lazy Susan | (2.40 ± 0.24) $10^{12}$ | 10 | (2.76 ± 0.04) $10^{12}$ |
| Thermal Channel | (2.52 ± 0.36) $10^{11}$ | 14 | (5.79 ± 0.07) $10^{11}$ |

agreement among the measurements with different HPGe detectors confirms the reliability of this methodological approach. The neutron flux was calculated using the data of 30 radioisotopes activated with different cross sections, obtaining a good agreement of the results. All the measurements and the analysis were performed with particular care to minimize the possible systematic errors and the individual results from 30 isotopes show that the remaining uncertainties for each irradiation channel are of the order of 10%. In particular, the approach described in this paper allows an absolute measurement of the neutron flux with good precision even through non-standard isotopes and target materials in different states of matter. This was possible thanks to the analysis of various activated isotopes and to the employment of different HPGe detectors in order to evaluate the real uncertainty associated with the measurements, taking into account the not negligible systematic error component.

agreement observed for Central Thimble, Rabbit Channel and Lazy Susan points out that the reactor core is well described in the simulations. On the contrary, the model should be improved in the region outside the reflector, because a significant discrepancy is recorded for the Thermal Channel.

## 5. Discussion

An absolute measurement of the integral neutron flux was performed by means of the neutron activation technique in four irradiation facilities of the TRIGA Mark II reactor of the University of Pavia. The γ-ray spectroscopy measurements were analyzed with the help of GEANT4 Monte Carlo simulations, that were crucial for a very accurate evaluation of the detection efficiency. The good

## References

Agostinelli, S., et al., 2003. Geant4: a simulation toolkit. Nucl. Instr. Meth. A 506, 250−303.
Borio di Tigliole, A., Cammi, A., Clemenza, M., Memoli, V., Pattavina, L., Previtali, E., 2010. Benchmark evaluation of reactor critical parameters and neutron fluxes distributions at zero power for the TRIGA Mark II reactor of the University of Pavia using the Monte Carlo code MCNP. Prog. Nucl. Energy 52 (5), 494−502.
Briesmeister, J., 2005. MCNP: a General Monte Carlo N-particle Transport Code. Los Alamos National Laboratory.
Clemenza, M., Cucciati, G., Maggi, V., Pattavina, L., Previtali, E., 2012. Radioactive fallouts as temporal makers for glacier ice cores dating. Eur. Phys. J. Plus 127, 68.
Evaluated Nuclear Data File (ENDF): http://www.nndc.bnl.gov/exfor/endf00.jsp http://www-nds.iaea.org/exfor/endf.htm.
Joint Evaluated Fission and Fusion File (JEFF): http://www.oecd-nea.org/dbdata/jeff/.
Merz, S., Djuricic, M., Villa, M., Böck, H., Steinhauser, G., 2011. Neutron flux measurements at the TRIGA reactor in Vienna for the prediction of the activation of the biological shield. Appl. Radiat. Isot. 69, 1621−1624.
Steinhauser, G., Merz, S., Stadlbauer, F., Kregsamer, P., Streli, C., Villa, M., 2012. Performance and comparison of gold-based neutron flux monitors. Gold Bull. 45, 17−22.